Solid-State Electronics Vol. 24, pp. 485–493, 1981
Printed in Great Britain.

0038-1101/81/060485-09$02.00/0
Pergamon Press Ltd.

NUMERICAL INVESTIGATION OF MESH SIZE CONVERGENCE RATE OF THE FINITE ELEMENT METHOD IN MESFET SIMULATION†

S. E. LAUX and R. J. LOMAX
Electron Physics Laboratory, Department of Electrical and Computer Engineering, The University of Michigan, Ann Arbor, MI 48109, U.S.A.

(*Received* 15 *August* 1980; *in revised form* 26 *September* 1980)

Abstract—The mesh size convergence rate of the finite element method in two-dimensional GaAs MESFET simulation has been investigated numerically. The equations governing MESFET operation and the finite element formulation of these equations are summarized. The presence of corner singularities at the gate contact endpoints is noteworthy, for such singularities are known to determine the convergence rate in linear model problems. The local potential and electron concentration solutions are obtained in the neighborhood of these singularities and used to estimate a lower bound on the convergence rate for the nonlinear problem. The rate of convergence of the MESFET problem is tabulated for three mesh sequences and discussed. The common source output characteristic of a 0.25 μm gate length GaAs MESFET is calculated and compared to the characteristic of a MESFET fabricated in our laboratory. Considerable discrepancy between the two is obtained; reasons for this are hypothesized.

NOTATION

A,B,C	non-zero constants
A_k,B_k	constants, possibly zero
D_n	field dependent electron diffusion constant
$\mathbf{E}$	electric field
E_0	constant in velocity-field relation
h	generalized mesh size parameter
$\bar{h}$	average mesh size parameter
h^*	average domain edge length
$J_D(J_D^h)$	continuum (discrete) drain current per unit gate width
$\mathbf{J}_n$	total electron particle current density
$n(n^h)$	continuum (discrete) electron concentration
N_d	doping concentration
n_i	intrinsic electron concentration
$\mathbf{n}$	unit normal vector
q	fundamental electronic charge
$Q(Q^h)$	continuum (discrete) total stored charge
$q\iint_\Omega$	$\int\int(N_d-n)\,dx\,dy$
(r,θ)	polar coordinates
t	time
$V(V^h)$	continuum (discrete) potential
V_{bi}	built-in potential (defined as negative)
V_0	constant potential value on contact
$\mathbf{v}_n$	field dependent electron velocity
v_{sat}	electron saturated velocity value
β	reciprocal thermal voltage $\simeq 38.67\ V^{-1}$ at 300 K
ϵ_s	semiconductor permittivity
ϵ_r	relative permittivity
$\zeta_n(\zeta_n^h)$	continuum (discrete) value of $e^{-\beta\phi n}$
ζ_{n0}	constant contact value of ζ_n
$\mu_n(\mu_{n0})$	field dependent (low field) electron mobility
$\phi_n(\phi_n^h)$	continuum (discrete) electron quasi-Fermi level
Ω	domain of simulation (or ohms when used as a unit)
Ω_1	local domain about a corner singularity
$\lvert\ \rvert$	magnitude
$\lVert\ \rVert$	norm (see Appendix for definition of norms)
∇	del vector operator
∇^2	Laplacian

1. INTRODUCTION

The mesh size convergence rate of the finite element method in two-dimensional GaAs MESFET simulation has been investigated numerically. The finite element formulation of the system of partial differential equations governing MESFET operation is summarized under the usual drift-diffusion approximation of electron transport. The MESFET geometry simulated is found to contain two corner singularities at the gate contact endpoints where unbounded potential and electron concentration gradients exist. Drain and source contact endpoints have bounded gradients due to the geometry simulated. Corner singularities can occur when a second order elliptic partial differential equation is solved in two-dimensions over a domain containing sharp "corners" and/or abrupt changes in boundary data along the domain edge. Such boundary problems have been treated in general in great depth[1, 2]. Corner singularities have been shown to determine the convergence rate of linear model problems[3] Chap. 8 and [4]: the existing mathematical theory for convergence rate of a nonlinear problem[5] cannot be directly applied due to the presence of unbounded gradients in the solution. Accordingly, the convergence rate for the nonlinear time independent MESFET problem will be estimated as bounded above by the approximation properties of the element shape functions, and bounded below by local solution behavior in the vicinity of corner singularities in a manner analogous to the result from linear model problems.

To determine the severity of the corner singularities, the governing differential equations are solved locally near the gate contact endpoints using Fourier series techniques. The results obtained are an extension of[6]. From this information, estimates of the convergence rate of the MESFET problem are made. Convergence estimates for the MOSFET problem biased so that the semiconductor surface is free of all mobile carriers are also possible (see Section 3). These estimates are tested by direct calculation of the rates of convergence for three sequences of finite element meshes. These sequences implement uniform mesh refinement, weak local mesh refinement, and strong local mesh refinement (see Section 5). The convergence of various discrete

†This work was supported by the National Science Foundation under Grant No. ENG 78-16973.

variables to their continuum values is measured as a function of mesh size in three norms: the L^2 (Euclidean) norm, the W_2^1, Sobolev norm, and the L^∞ (maximum) norm (see Appendix for definition of norms). The variables investigated are potential V, electron concentration n, electron quasi-Fermi level ϕ_n, drain current/gate width J_D, and total stored charge Q. A 0.25 μm gate length GaAs MESFET is simulated. The common source output characteristic obtained is compared to the characteristic of a MESFET fabricated in our laboratory. There is considerable discrepancy; reasons for this will be hypothesized.

Section 2 presents the governing partial differential equations, the MESFET simulated, and the formulation of the discrete equations using the finite element method. Section 3 derives the analytic form of the potential and electron concentration solutions at the gate contact endpoints of the MESFET. Section 4 estimates the convergence rate of the finite element method for this nonlinear problem. The MESFET convergence experiments for the three mesh sequences are summarized in Section 5. Section 6 compares the simulated and experimentally measured MESFET common source output characteristics, and lists reasons for their marked deviation. Section 7 presents conclusions.

2. GOVERNING EQUATIONS, MESFET SIMULATED, AND DISCRETE FORMULATION

The following system of partial differential equations and auxiliary equations are used to model MESFET operation. The partial differential equations are

$$-\nabla\cdot(\epsilon_s\nabla V) = q(N_d - n) \text{ (Poisson's equation)} \quad (1)$$

$$q\frac{\partial n}{\partial t} = \nabla\cdot\mathbf{J}_n \text{ (Electron Current Continuity equation).} \quad (2)$$

The auxiliary equations are

$$\mathbf{J}_n = q\mu_n n\mathbf{E} + qD_n\nabla n \quad (3)$$

$$= -q\mu_n n_i e^{\beta(V-\phi_n)}\nabla\phi_n \quad (4)$$

$$= qD_n n_i e^{\beta V}\nabla\zeta_n \quad (5)$$

$$\mathbf{E} = -\nabla V \quad (6)$$

$$\mathbf{v}_n = -\mu_n\mathbf{E}. \quad (7)$$

The following assumptions are implicit in eqns (1)–(7):

1. A drift-diffusion description of electron transport. This ignores non-local effects such as electron velocity overshoot, and is a major assumption.
2. The Einstein relation $\mu_n/D_n = \beta$.
3. No trap induced generation-recombination, impact ionization, or fixed charge other than that included in N_d.
4. Neglect of holes.
5. Scalar diffusion constant D_n and mobility μ_n.

To obtain eqn (4) from eqn (3), the substitution $n = n_i e^{\beta(V-\phi_n)}$ is used. To obtain eqn (5) from eqn (3), the substitution $n = n_i e^{\beta V}\zeta_n$ is used.

Three types of boundary conditions are used. Along ohmic conducting surfaces, Dirichlet boundary conditions are used. The boundary potential is the applied potential; the boundary electron concentration is determined by assuming charge neutrality. Along rectifying conducting surfaces, Dirichlet boundary conditions are used. The boundary potential is the applied potential plus the built-in potential; the boundary electron concentration depends on the gate-source bias potential. In reverse bias, a balance between diffusion and thermionic current flow determines the electron concentration[7]. In forward bias, thermionic current flow dominates and determines the electron concentration[8, 9]. Along nonconducting surfaces, Neumann boundary conditions are used. On assuming zero permittivity external to the MESFET and no trapped surface charge, appropriate boundary conditions are $\nabla V\cdot\mathbf{n} = \mathbf{J}_n\cdot\mathbf{n} = 0$, where $\mathbf{n}$ is the unit vector normal to the surface.

The cross section of the 0.25 μm gate length GaAs MESFET to be modeled is shown in Fig. 1. (source, gate, and drain are marked S, G, D, respectively). The active layer is uniformly doped $N_d = 1.0\times10^{17}\,\text{cm}^{-3}$ and is 0.25 μm thick; the gate width is 125 μm. The actual source-drain spacing is 5 μm; however, only a region 1 μm long centered about the gate is simulated in two-dimensions. This is the device region delineated by the dotted lines S' and D' in Fig. 1. The ohmic effects of the contact regions of Fig. 1 are added in after the two-dimensional simulation is complete. This assumes charge neutrality and uniform orthogonal current flow at the S' and D' lines and will be valid only if the gate depletion layer stays well away from S' and D'. This will occur for $S'-G$ and $D'-G$ biases below approximately 5–6 V

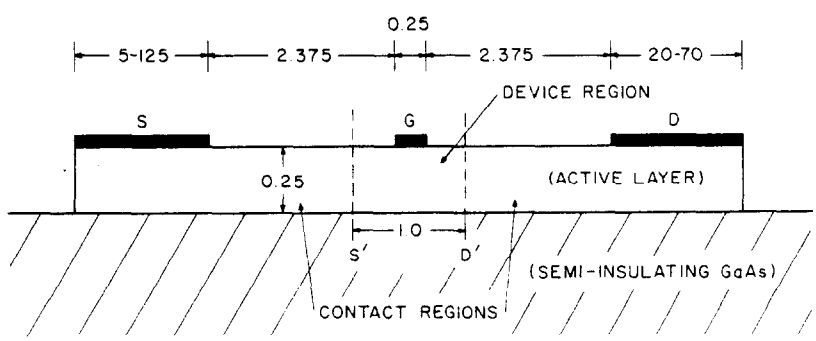

Fig. 1.

(not including built-in potential). The semi-insulating substrate is assumed ideal, and hence Neumann boundary conditions are imposed along the active layer—semi-insulating interface.

GaAs material parameters are taken as follows:

1. $\epsilon_r = 12.5$.
2. $$|v_n| = \frac{\mu_{n0}|\mathbf{E}| + v_{sat}(|\mathbf{E}|/E_0)^4}{1 + (|\mathbf{E}|/E_0)^4}$$

with

$$\mu_{n0} = 5000\ \text{cm}^2/V \cdot s,\ v_{sat} = 1 \times 10^7\ \text{cm/s},$$

and

$$E_0 = 2.691 \times 10^3\ \text{V/cm}.$$

3. $V_{bi} = -0.805$ V for the gate junction.

The governing equations are solved using the finite element method. Linear shape functions defined on triangular finite elements are used to describe the spatial variation of V and ϕ_n. This results in exponential electron concentration spatial variation; numerically induced negative electron concentrations are impossible. The discrete MESFET solution so obtained is electron current and electric flux density conservative, both locally (each finite element) and globally, independent of mesh size. The details are given in[10, 11] except for the use of quasi-Fermi levels instead of electron concentration. Although the resulting program does perform a true transsient calculation, unless otherwise noted, $\partial n/\partial t = 0$ will be assumed in eqn (2).

3. ANALYTIC FORM OF POTENTIAL AND ELECTRON CONCENTRATION AT GATE ENDPOINTS

In this section, eqns (1) and (2) will be solved locally near the MESFET gate endpoints to determine the severity of the singularity present. The technique is also applicable to MOSFET's biased so that the semi-conductor surface is fully depleted of mobile carriers. The singularity problem has been treated in general[1] and in the context of semiconductor modeling[6]. The following treatment expands on[6] by solving eqns (1) and (2) simultaneously under the assumption of no time variation ($\partial n/\partial t = 0$ in eqn 2) and zero permittivity outside the device region. Since the depletion approximation $n \ll N_d$ is an excellent assumption in the gate depletion region, the problem reduces to:

Solve

$$\nabla^2 V = -\frac{q}{\epsilon_s} N_d \tag{8}$$

and

$$\nabla \cdot (qD_n n_i e^{\beta V} \nabla \zeta_n) = 0 \tag{9}$$

simultaneously in the domain $\Omega_1 = \{(r, \theta) | 0 < r < \delta,\ 0 < \theta < \alpha\pi\}$ subject to the boundary conditions

$$V(r, \theta = 0) = V_0,\ \zeta_n(r, \theta = 0) = \zeta_{n0} \tag{10}$$

$$\left.\frac{\partial V}{\partial \theta}\right|_{\theta = \alpha\pi} = \left.\frac{\partial \zeta_n}{\partial \theta}\right|_{\theta = \alpha\pi} = 0 \tag{11}$$

$$|V| < \infty,\ |\zeta_n| < \infty \text{ in } \Omega_1. \tag{12}$$

Here δ is some fixed small positive number, and V_0, ζ_{n0} are constant boundary values along the contact $0 < r < \delta$, $\theta = 0$. The domain is chosen to have a variable angle $\alpha\pi$ (in the MESFET, $\alpha = 1$), and to use eqn (5) $\mathbf{J}_n$ in eqn (9). The depletion approximation has decoupled eqns (1) and (2). Equation (8) can be solved in Ω_1, then eqn (9) is solved using the resulting potential solution from eqn (8).

A Fourier series analysis solution following[4] is used to solve both eqns (8) and (9). Since each equation is solved similarly, the potential solution will be given, then the solution for ζ_n will be outlined. The solution to eqn (8) subject to eqns (10)–(12) is

$$V(r, \theta) = V_0 + Ar^{1/2\alpha} \sin\frac{\theta}{2\alpha} + o(r^{1/2\alpha}) \tag{13}$$

for $\alpha > 1/4$,

$$V(r, \theta) = V_0 + Ar^2 \sin 2\theta + Br^2 \ln r \sin 2\theta + o(r^2) \tag{14}$$

for $\alpha = 1/4$, and

$$V(r, \theta) = V_0 + Ar^2 \sin 2\theta + o(r^2) \tag{15}$$

for $0 < \alpha < 1/4$. As indicated in Section 4, only $\alpha > 1/2$ is of concern. Equation (13) can be differentiated formally[1] to yield

$$\nabla V = \left(\frac{A}{2\alpha} r^{(1/2\alpha)-1} \sin\frac{\theta}{2\alpha}, \frac{A}{2\alpha} r^{(1/2\alpha)-1} \cos\frac{\theta}{2\alpha}\right).$$

Since $\alpha > 1/2$, r has a negative exponent and so the electric field is unbounded as $r \to 0$. Consistent with the velocity-field characteristic of Section 2 and the Einstein relation, $D_n \to (V_{sat}/\beta|\mathbf{E}|)$ as $|\mathbf{E}| \to \infty$ and then for small r

$$D_n = \frac{v_{sat}}{\beta} \frac{2\alpha}{A} r^{1-(1/2\alpha)}.$$

Also as $r \to 0$, $e^{\beta V} \approx e^{\beta V_0}$ and eqn (9) becomes

$$\nabla \cdot \left(q \frac{v_{sat}}{\beta} \frac{2\alpha}{A} n_i e^{\beta V_0} r^{1-(1/2\alpha)} \nabla \zeta_n\right) = 0. \tag{16}$$

Taking into account eqns (10) and (11), eqn (16) can be solved as follows. Let

$$\zeta_n(r, \theta) - \zeta_{n0} = \sum_{j=0}^{\infty} u_{2j+1}(r) \Psi_{2j+1}(\theta) \tag{17}$$

with $\Psi_{2j+1}(\theta) = \sqrt{(2/\alpha\pi)} \sin[(2j+1)\theta/2\alpha]$. Using eqn (17) in eqn (16) and the orthogonality properties of the Ψ_{2j+1} yields

$$\frac{d^2u_k}{dr^2}+\frac{1}{r}\left(2-\frac{1}{\alpha}\right)\frac{du_k}{dr}-\left(\frac{k}{2\alpha}\right)^2\frac{1}{r^2}u_k=0,\ k\ \text{odd}. \quad (18)$$

The solution to eqn (18) is

$$u_k(r)=A_kr^{S_{k1}}+B_kr^{S_{k2}} \quad (19)$$

where

$$S_{k1,2}=\frac{-\left(1-\frac{1}{2\alpha}\right)\pm\sqrt{\left(\left(1-\frac{1}{2\alpha}\right)^2+4\left(\frac{k}{2\alpha}\right)^2\right)}}{2}. \quad (20)$$

The dominant term of eqn (17) as $r\to 0$ is sought subject to $|\zeta_n|<\infty$ in Ω_1. Using eqns (19)–(20), this result is

$$\zeta_n(r,\theta)=\zeta_{n0}+Ar^{S_{\min}}\sin\frac{\theta}{2\alpha}+o(r^{S_{\min}}) \quad (21)$$

with

$$S_{\min}=\frac{-\left(1-\frac{1}{2\alpha}\right)+\sqrt{\left(\left(1-\frac{1}{2\alpha}\right)^2+\frac{1}{\alpha^2}\right)}}{2}. \quad (22)$$

For $\alpha>1/2$, $S_{\min}<1$ therefore the potential and ζ_n have unbounded gradients as $r\to 0$. Their local behavior is given by eqns (13), (21) and (22). The local electron concentration and electron quasi-Fermi level solutions can be constructed from eqns (13) and (21).

4. ESTIMATE OF CONVERGENCE OF THE FINITE ELEMENT METHOD

The mesh size convergence rate of the finite element method for elliptic partial differential equations in the presence of corner singularities has been well documented in two areas. Firstly, convergence rates for linear model problems have been derived rigorously[3, 4], and verified computationally[4, 12]. Secondly, a general theory for convergence of nonlinear problems exists for the case when gradients remain bounded[5]. Unfortunately, neither case applies to the time independent MESFET problem. Accordingly, in order to have some reference to compare to the computationally measured convergence rate of eqns (1) and (2), the convergence rate for this nonlinear problem with unbounded gradients will only be estimated. The convergence rate is hypothesized to be estimated from above by the approximation properties of the linear shape functions used (optimal order convergence), and from below by local solution behavior in the vicinity of corner singularities in a manner analogous to linear model problem results to be described below.

Consider a sequence of regular triangulations of domain Ω parameterized by a single (normalized) mesh size variable h with $0<h<1$. For linear shape functions on triangular elements, a sequence of triangulations is *regular* (or *non-degenerate* or in compliance with a *uniformity condition*) if all vertex angles of all triangular elements are bounded away from zero as $h\to 0$. Following[4], for a linear elliptic problem with the coefficient of the Laplacian bounded away from zero, and if $u(u^h)$ represents the continuum (discrete) solution to the second order problem, then for linear shape functions in two-dimensions:

$$u\in W_2{}^k(\Omega)\Rightarrow\|u-u^h\|_{w_2{}^1(\Omega)}\leqq Ch^{k-1}, \quad (23)$$

$$\|u-u^h\|_{L^2(\Omega)}\leqq Ch^{2(k-1)} \quad (24)$$

valid for $1\leqq k\leqq 2$ (see Appendix for definition of norms). Equations (23) and (24) apply as written to the potential solution in Ω_1 given in Section 3: this local behavior of V is assumed to be an estimate for the convergence behavior of V over the entire domain Ω. Equations (23) and (24) are not strictly applicable to the ζ_n solution in Ω_1 given in Section 3. The convergence rate of eqn (9) lies outside the conventional theory since the Laplacian coefficient contains D_n which tends to zero in Ω_1 as $r\to 0$. This major stumbling block aside, eqns (23)–(24) will also be used to estimate the convergence rate of ζ_n over Ω_1 and Ω. The upper estimate of convergence assumes the element shape function limits convergence rate: this is the case $k=2$ in eqns (23) and (24) and will be referred to as optimal order dominant (OOD) convergence. The lower estimate of convergence uses the severity of the singularities in V and ζ_n to estimate convergence; this will be referred to as corner singularity dominant (CSD) convergence. The following paragraph extracts the k value to be used in eqns (23)–(24) for CSD convergence estimates.

For the MESFET of Section 2, the simulated region Ω between S' and D' contains six "corners"—four are the 90° polygon corners, and two are the present at the endpoints of the gate contact. For the polygon corners, $\alpha=1/2$. The electric field is bounded as $r\to 0$. Both Poisson's equation and the electron current continuity equation have leading coefficients bounded away from zero, and eqns (23) and (24) apply to V and ζ_n directly near the four corners. If these were the only corners (i.e. no gate), then[5] guarantees optimal order convergence over the whole domain Ω. Hence, these four corners are reasonably taken as having no detrimental effect on convergence properties of the problem. For the gate contact endpoints, $\alpha=1$. From Section 3, $V=V_0+Ar^{1/2\alpha}\sin(\theta/2\alpha)+\cdots$, therefore $V\in W_2^{(1/2\alpha)+1+\delta}(\Omega)$, where δ is an arbitrarily small positive number. Thus, $k=(1/2\alpha)+1-\delta\approx(1/2\alpha)+1$, and from eqns (23) and (24)

$$\|V-V^h\|_{w_2{}^1}\leqq Ch^{1/2\alpha}=Ch^{1/2} \quad (25)$$

$$\|V-V^h\|_{L^2}\leqq Ch^{1/\alpha}=Ch. \quad (26)$$

From Section 3, $\zeta_n=\zeta_{n0}+Ar^{S_{\min}}\sin(\theta/2\alpha)+\cdots$ therefore $\zeta_n\in W_2{}^{S_{\min}+1-\delta}(\Omega)$, $k=S_{\min}+1-\delta\approx S_{\min}+1$. Thus

$$\|\zeta_n\zeta_n{}^h\|_{w_2{}^1}\leqq Ch^{S_{\min}}=Ch^{0.309} \quad (27)$$

$$\|\zeta_n-\zeta_n{}^h\|_{L^2}\leqq Ch^{2S_{\min}}=Ch^{0.618}. \quad (28)$$

These are the CSD convergence estimates for V and ζ_n.

Estimates are still needed for ϕ_n, n, Q, and J_D. In the spirit of eqns (25)–(28), and without rigorous proof, the following CSD estimates seem reasonable:

$$\|n - n^h\|_{W_2^1} \leqq Ch^{0.309} \tag{29}$$

$$\|n - n^h\|_{L^2} \leqq Ch^{0.618} \tag{30}$$

$$\|\phi_n - \phi_n{}^h\|_{W_2^1} \leqq Ch^{0.309} \tag{31}$$

$$\|\phi_n - \phi_n{}^h\|_{L^2} \leqq Ch^{0.618} \tag{32}$$

$$|Q - Q^h| \leqq Ch^{\gamma}, \quad \gamma \geqq 0.618 \tag{33}$$

$$|J_D - J_D{}^h| \leqq Ch^{\sigma}, \quad \sigma \geqq 0.309 \tag{34}$$

It is difficult to determine if eqns (29)–(34) are sharp error bounds. Equations (33)–(34) are particularly suspect since the definitions of Q and J_D involve integration which may well increase the rates of convergence of Q and J_D. Equations (29)–(34) therefore represent pessimistic error bounds. For OOD bounds, substitute 1.0 for 0.309 or 1/2, and 2.0 for 0.618 or 1 in eqns (25)–(34). Maximum norm convergence of V, ϕ_n, and n is estimated to lie between L^2 and W_2^1 bounds for CSD and OOD convergence [5].

Each norm in eqns (25)–(34) has a single convergence rate exponent associated with it as determined by the governing equations and domain Ω. If corner singularities limit convergence rate then CSD estimates should be close to numerically measured rates; if the degree of shape function approximation limits convergence rate the OOD estimates should be close to numerically measured rates. In every case, faster convergence is allowed for due to the inequality present in eqns (25)–(34). Additionally, eqns (25)–(34) apply only for linear shape functions defined on mesh sequences which are singly parameterized by h. For sufficient local mesh refinement (resulting in a mesh which may not be singly parameterized, see Section 5) or by inclusion of singular shape functions, restoration of OOD convergence rates is expected [4]. For the case of local mesh refinement this is verified in Section 5.

5. NUMERICAL EXPERIMENTS ON MESFET CONVERGENCE

Three sequences of finite element meshes were used to examine the convergence of the system of eqns (1) and (2) using linear shape functions for the variables V and ϕ_n. Unless otherwise specified, the MESFET is biased at a constant $V_{D'S'} = 0.2$ V, $V_{GS'} = 0$ V. As seen in Section 6, this is in the region of stable differential negative resistance. Define the average mesh size parameter $\bar{h}$ as

$$\bar{h} \triangleq \left(\frac{\text{area}(\Omega)}{NE}\right)^{1/2} \propto NE^{-1/2} \tag{35}$$

where NE = the number of finite elements in the mesh. The three mesh sequences are described as follows:

1. *Sequence* 1. This sequence of meshes consists of four meshes starting with the triangulation of Fig. 2. To obtain the next mesh in the sequence, the number of elements is quadrupled ($\bar{h}$ is halved) by connecting midpoints of the three element sides. Each of the four newly created triangular elements is similar to the original element; therefore, vertex angles are bounded away from zero as required. The remaining two meshes in the sequence are obtained similarly. These meshes are referred to as M1.1, M1.2, M1.3, and M1.4 (the first digit means Sequence 1, the second digit orders the meshes from coarse to fine). Sequence 1 implements uniform mesh refinement, indicating local mesh size is decreasing at a uniform rate over the entire domain as the meshes are examined in sequence.

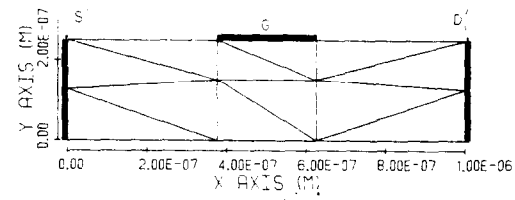

Fig. 2.

2. *Sequence* 2. This sequence of meshes consists of five meshes starting with the triangulation of Fig. 3. This is mesh M2.1. The next four meshes are obtained as for Sequence 1, with two additions. The first addition is that an attempt is made to decrease the mesh size faster near the gate due to the anticipated singularities. This is done by no longer refining between edge midpoints, but rather dividing edges into two segments with length ratios $1{:}R$, $1 \leqq R \lesssim 2$ so that the smaller triangle is oriented nearest the gate. The second addition is to reduce the mesh by different factors in the x- and y-directions. The refinement is accomplished as follows: (1) transform mesh M2.1 into a 6×3 regular nodal mesh, (2) refine this mesh into a $NX \times NY$ nodal mesh (in this case 9×5 to obtain M2.2), (3) transform the new mesh back to the original geometry, (4) reconnect nodes with segments to form a valid triangulation and (5) perturb the mesh as previously described to force smaller elements near the gate. The remaining meshes M2.3, M2.4, and M2.5 are obtained similarly; M2.5 is shown in Fig. 4. Sequence 2

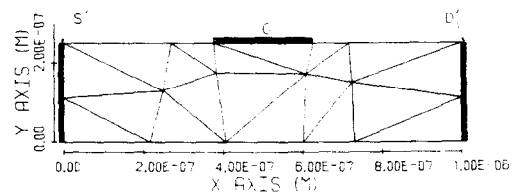

Fig. 3.

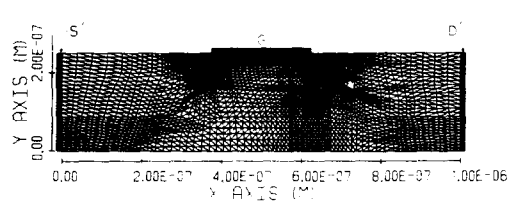

Fig. 4.

implements weak local mesh refinement, indicating local mesh size decreases up to 2.5 times faster near the singularities than near S' and D' as the meshes are examined in sequence.

3. *Sequence* 3. This sequence of meshes consists of two meshes, starting with M2.2 = M3.1. Mesh M3.2 is obtained by using the structure of M2.5 immediately adjacent to the gate contact endpoints, and then smoothly blending this fine mesh structure into the coarser mesh structure of M2.3 within a distance of $\sim 0.05\,\mu$m of the gate. Mesh M3.2 is shown in Fig. 5. Sequence 3 implements strong local mesh refinement, indicating local mesh size decreases much faster (here 6.6 times) near the singularities than near S' and D' as the meshes are examined in sequence.

Each Sequence 1–3 can be considered to be singly parameterized by $\bar{h}$; this is true for any finite sequence of meshes. In the limit $\bar{h} \to 0$, Sequence 1 is clearly still singly parameterized; for Sequences 2–3 this may not be the case. Hence, Sequence 1 will best measure the convergence rate of eqns (1) and (2). Table 1 summarizes the three mesh sequences.

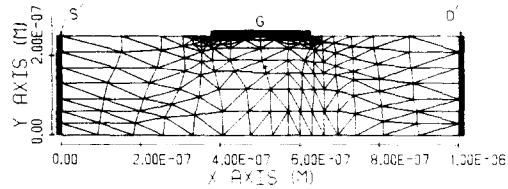

Fig. 5.

Table 2 summarizes the results of the convergence experiments. Error norms of the form (25)–(34) are calculated for the three mesh sequences, and the exponent σ in the expression

$$\|u - u^h\| \leqq C(\bar{h})^{\sigma} \tag{36}$$

is tabulated. The CSD and OOD exponent values of Section 4 are also tabulated for comparison. Note σ could be tabulated against h_{min} or h_{max} (see Table 1 for definitions). Since Sequence 1 is singly parameterized, the choice is irrelevant. However, for Sequences 2 or 3, the entries in Table 2 will change somewhat if this is

Table 1. Mesh specifications

Quantity	Mesh Name									
	M1.1	M1.2	M1.3	M1.4	M2.1	M2.2	M2.3	M2.4	M2.5	M3.2
No. of nodes	17	45	117	425	17	45	136	495	1885	194
No. of elements	12	48	192	768	20	84	294	996	3584	328
No. of S'/G/D' nodes	3	5	9	17	3	5	9	17	33	27
No. nodes, x-direction (NX)	4	7	13	25	4	7	13	25	49	*
No. nodes, y-direction (NY)	5	9	17	33	5	9	17	33	65	*
Min. mesh size in μm (h_{min})	0.1000	0.0500	0.0250	0.0125	0.0754	0.0380	0.0190	0.0050	0.0025	0.0025
Max. mesh size in μm (h_{max})	0.3953	0.1976	0.0988	0.0494	0.2922	0.1459	0.0729	0.0776	0.0388	0.1552
$\bar{h}$ [eqn (35)] in μm	0.1443	0.0722	0.0361	0.0180	0.1118	0.0625	0.0334	0.0167	0.00835	0.0276
h_{max}/h_{min}	3.95	3.95	3.95	3.95	3.88	3.84	3.83	15.52	15.52	62.08

* : Not applicable, since M3.2 not topologically equivalent to a uniform rectangle nodal mesh.

Table 2. Convergence rate exponent σ [defined in (36)]

Norm:	Convergence Rate Between Meshes							Section IV Estimates	
	M1.1/M1.2	M1.2/M1.3	M1.3/M1.4	M2.1/M2.2	M2.2/M2.3	M2.3/M2.4	M3.1/M3.2	CSD	OOD
$\|V-V^h\|_{L^2}$	0.97	0.97	1.04	1.12	1.49	1.73	2.13	1	2
$\|\phi_n-\phi_n^h\|_{L^2}$	0.76	0.84	1.07	0.83	1.01	1.36	2.48	0.618	2
$\|n-n^h\|_{L^2}$	0.37	1.35	1.25	0.63	1.97	1.94	1.87	0.618	2
$\|V-V^h\|_{W_2^1}$	0.51	0.65	0.66	0.65	0.83	0.84	1.06	0.5	1
$\|\phi_n-\phi_n^h\|_{W_2^1}$	0.06	0.12	0.32	0.00	0.76	0.49	1.85	0.309	1
$\|n-n^h\|_{W_2^1}$	0.28	0.72	1.25	0.20	0.87	1.18	0.77	0.309	1
$\|V-V^h\|_{L^\infty}$	0.29	0.48	0.62	0.70	0.80	1.13	2.64	0.5–1	1–2
$\|\phi_n-\phi_n^h\|_{L^\infty}$	0.02	0.03	0.04	0.06	0.34	0.59	2.28	0.309–0.618	1–2
$\|n-n^h\|_{L^\infty}$	−0.36	0.62	0.77	0.18	1.44	1.17	1.87	0.309–0.618	1–2
$\|J_D-J_D^h\|$	0.00	1.65	2.26	0.78	0.71	2.19	2.23	$\geq$0.309	$\geq$1
$\|\phi-\phi^h\|$	0.02	0.98	1.23	0.62	1.64	1.86	2.25	$\geq$0.618	$\geq$2

done. The use of $\bar{h}$ is consistent with other work[4, 12]; if h_{min} or h_{max} are used the overall conclusions drawn from Table 2 remain unchanged (see next paragraph). Norm calculation requires knowledge of the continuum solution to eqns (1) and (2), which for practical reasons is taken to be the solution to eqns (1) and (2) on mesh M2.5. The validity of this convention merits brief discussion. M2.5 is twice as refined as any other mesh used (with the exception of M3.2 within 0.005 μm of the gate endpoints). L^2 and W_2^1 error norm values calculated for the solution on M2.3 with either M2.4 or M2.5 as the "continuum" solution differed at most by 25%, and typically 12%. This reduced sensitivity was anticipated due to the smoothing effect of integrations performed in norm calculation, and supports the sufficiency of halving element sizes for continuum solution definition. However, examination of V and ζ_n solutions on M2.5 near the gate endpoints shows V in excellent agreement with eqn (13) for $\alpha = 1$, but ζ_n in marked disagreement with eqn (21) for $S_{min} = 0.309$. The discrepancy in ζ_n arises because the assumption $e^{\beta V} \approx e^{\beta V^0}$ made prior to eqn (16) only becomes valid within 10% for $r \leqq 0.0038$ Å. This is an impractical dimension beyond the validity of the equations. Accordingly, norms involving $(\phi_n - \phi_n^h)$ cannot indicate true asymptotic behavior; $(V - V^h)$ norms are not limited by this difficulty. Furthermore, $(n - n^h)$ and $(Q - Q^h)$ norms are unaffected since their values are weighted away from the singularities due to the depletion region; lack of asymptotic ζ_n values should not strongly affect $(J_D - J_D^h)$ norms.

Three conclusions are evident from Table 2. Firstly, when strict uniform mesh refinement is used as in Sequence 1, suboptimal convergence rates of V, ϕ_n, and n are observed. Reduced convergence in V or ϕ_n is particularly evident; convergence of n is less hampered due to the presence of the depletion region near the gate which strongly weights the $\|n - n^h\|_{L^2}$, $\|n - n^h\|_{W_2^1}$, and $\|n - n^h\|_{L^\infty}$ norms away from the gate contact. The CSD estimates for V, ϕ_n, and n are generally seen to be pessimistic, but reasonably good, in predicting convergence rate of Sequence 1. Secondly, the use of local mesh refinement does restore V, ϕ_n and n convergence to near optimal levels. Sequence 2 is somewhat suboptimal due to the weak local refinement process used. Convergence of Sequence 3 is essentially OOD as a result of the strong local mesh refinement near the gate endpoints of the MESFET problem. Thirdly, for all mesh sequences, $|Q - Q^h|$ and especially $|J_D - J_D^h|$ converged much more rapidly than expected. The reason for this is unclear; however, it is hypothesized this is at least partly due to the current and electric flux density conservative formulation used to solve eqns (1) and (2).

Figure 6 shows $\|V - V^h\|_{L^2}$ and $\|V - V^h\|_{W_2^1}$ vs reciprocal average mesh size $(\bar{h})^{-1}$ and indicates the relative ability of the three mesh sequences in error reduction. Mesh M2.1 (Fig. 3) places less constraint on the solution than mesh M1.1 (Fig. 2) near the gate contact and results in decreased initial norm values for Sequence 2 over Sequence 1. This causes Sequences 2 and 3 to lie well below Sequence 1 in Fig. 6. Figure 6

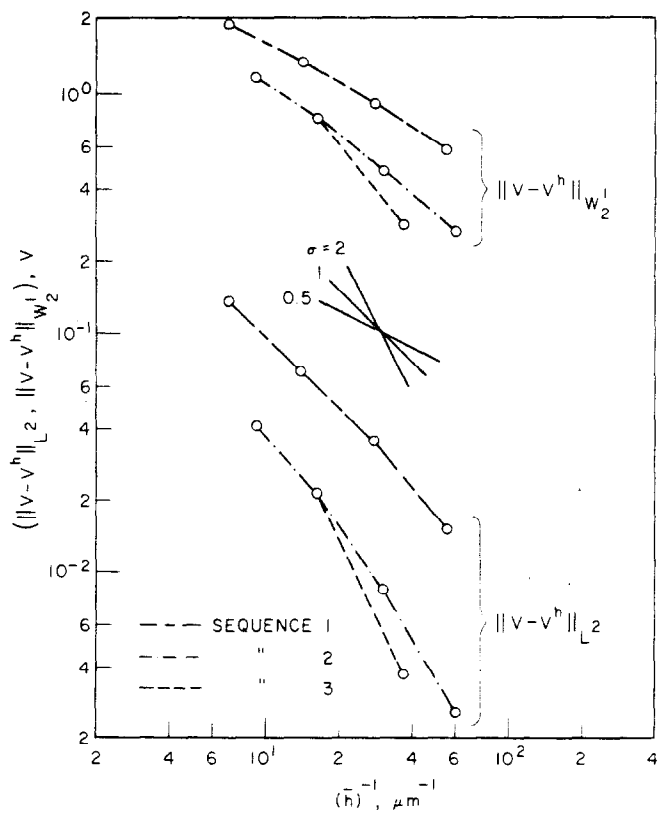

Fig. 6.

shows the CSD and OOD slopes (σ value) for the $\|V - V^h\|_{L^2}$ norm (1.0 and 2.0, respectively) and for the $\|V - V^h\|_{W_2^1}$ norm (0.5 and 1.0, respectively) for comparison. The large separation between $\|V - V^h\|_{L^2}$ and $\|V - V^h\|_{W_2^1}$ values in Fig. 6 depends on the normalizing distance used (see Appendix for normalization used). For normalizing distance h^* sufficiently small, the $\|V - V^h\|_{W_2^1}$ values in each sequence become identical to the $\|V - V^h\|_{L^2}$ values for finite mesh size $\bar{h}$. This masks the lower order behavior of $\|V - V^h\|_{W_2^1}$. The normalization used for finite $\bar{h}$ must assure the $\|V - V^h\|_{W_2^1}$ calculation is dominated by the derivative terms in the W_2^1 norm definition. The normalization used here does have this property for $\|V - V^h\|_{W_2^1}$, as well as for $\|\phi_n - \phi_n{}^h\|_{W_2^1}$ and $\|n - n^h\|_{W_2^1}$.

6. D.C. COMMON SOURCE CHARACTERISTICS

The d.c. common source characteristic of the simulated MESFET described in Section 2 is shown in Figs. 7 and 8. Figure 7 shows the characteristics before the addition of $S - S'$ and $D - D'$ parasitic resistances. Note for $0.2 \leqq V_{D'S'} \leqq 0.3\,V$ and $V_{GS'} \geqq -0.5$ V, a region of stable differential negative resistance is seen. The mesh dependence of this region has been previously described in[13]. Figure 8 shows the same results after the addition of $S - S'$ and $D - D'$ resistances of 0.34 Ω cm. This value is chosen to fit the triode region output conductance g_D of the simulated device to the MESFET fabricated in our laboratory[14, 15]. This fabricated device is shown dotted in Fig. 8. Significant differences are seen between the two sets of characteristics. Some of the reasons felt to be responsible for the discrepancies are:

1. The validity of all assumptions, particularly the drift-diffusion approximation, must be questioned. True energy/momentum balance simulations in two-dimensions are currently prohibitively expensive[6].

2. The large parasitic resistances necessary to fit low field output conductances signal some defect in material parameters used in the simulation, or some unmodeled effect present in the active device region. This problem has been noted by others[17, 18]. Simplified resistance calculations[19] and two-dimensional modeling of $S - S'$ and $D - D'$ regions by the authors do not justify these large parasitic resistances.

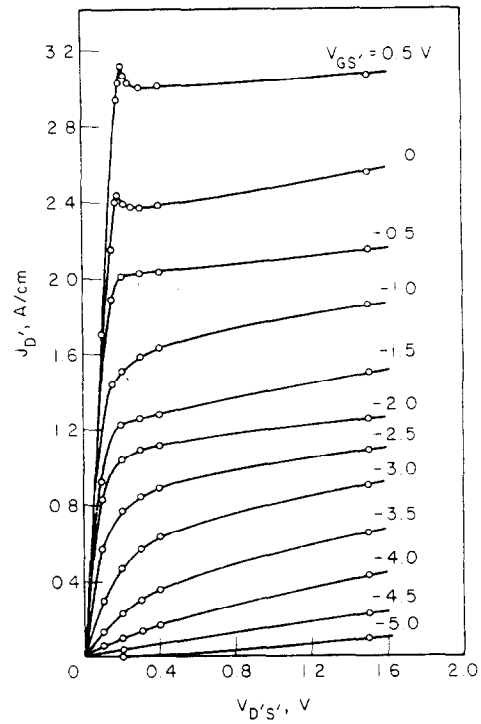

Fig. 7.

3. The extremely low (often negative) output conductance of the laboratory device at high drain bias seems in conflict with other modeling efforts[16, 20, 21], not just this one. Semi-insulating substrate-active layer effects[22] and non-isothermal conditions within the device[23] are two unmodeled effects known to be operational in the MESFET for this bias region.

7. CONCLUSIONS

A 0.25 μm gate length GaAs MESFET is numerically simulated in two dimensions. The local potential and ζ_n

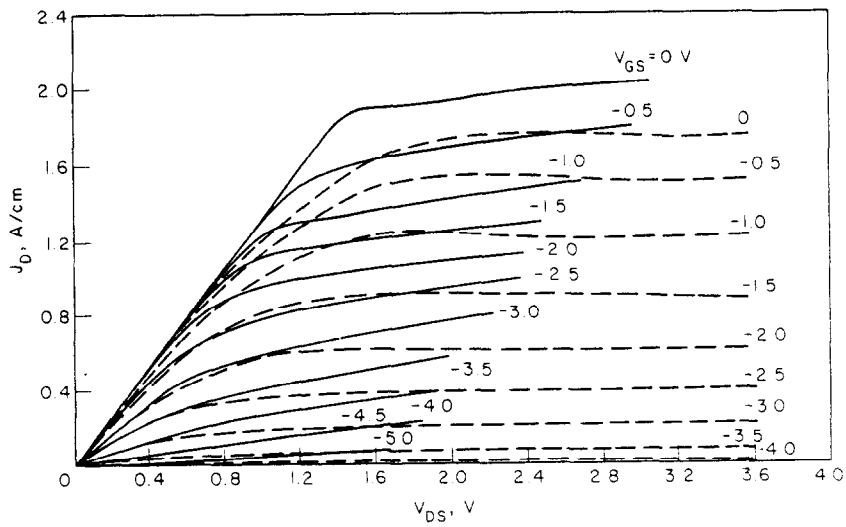

Fig. 8.

solutions near the gate contact endpoints are derived and given by eqns (13), (21) and (22). The mesh size convergence rate of the time independent system of partial differential equations governing MESFET operation is estimated to lie between CSD (corner singularity dominant) and OOD (optimal order dominant) convergence extremes for mesh sequences parameterized by a single average mesh size value $\bar{h}$. Three mesh sequences implementing uniform refinement, weak local refinement, and strong local refinement are used to measure the convergence rate. The tabulated results of Table 2 indicate suboptimal convergence rates are obtained unless local mesh refinement is used (singular shape functions should give the same results, see [4]). Both drain current density and stored charge converged faster than anticipated. A comparison is made between the common source output characteristics of the simulated MESFET and a MESFET fabricated in our laboratory [14, 15]. Reasons for the lack of agreement between the characteristics are hypothesized in Section 6.

Acknowledgements—The laboratory fabrication and characterization work of Dr. T. N. Jackson is gratefully acknowledged.

REFERENCES

1. R. S. Lehman, *J. Math. Mech.* **8**, 727 (1959).
2. V. A. Kondrat'ev, *Trans. Moscow Math. Soc.* **16**, 227 (1967).
3. I. Babuska and A. K. Aziz, *The Mathematical Foundations of the Finite Element Method with Applications to Partial Differential Equations* (Edited by A. K. Aziz). Academic Press, New York (1972).
4. G. Strang and G. J. Fix, *An Analysis of the Finite Element Method*. Prentice-Hall, Englewood Cliffs, New Jersey (1973).
5. R. Rannacher, Habilitationsschrift, Der Rheinischen Friedrich-Wilhelms-Universität zu Bonn (1978).
6. J. A. Lewis and E. Wasserstom, *Bell Syst. Tech. J.* **49**, 1183 (1970).
7. C. R. Crowell and M. Beguwala, *Solid-St. Electron.* **14**, 1149 (1971).
8. E. H. Rhoderick *J. Phys. D: Appl. Phys.* **5**, 1920 (1972).
9. E. H. Rhoderick, *Metal-Semiconductor Contacts*. Clarendon Press, Oxford (1978).
10. J. J. Barnes and R. J. Lomax, *IEEE Trans Electron Dev.* **ED-24**, 1082 (1977).
11. R. J. Lomax, Technical report on application of the finite element method to semiconductor device modeling, Report No. UM-EPL-014289-T1, NTIS Accession No. PB287729/AS. Electron Physics Laboratory, The University of Michigan, Ann Arbor (1978).
12. R. E. Bank and A. H. Sherman, *Symp. Sparse Matrix Computations*, Knoxville, Tennessee, p. 62 (1978).
13. S. E. Laux and R. J. Lomax, *IEEE Trans Electron Dev.* **ED-28**, 120 (1981).
14. T. N. Jackson and N. A. Masnari, *Proc.* 1979 *Int. Electron Devices Meeting*, 58 (1979).
15. T. N. Jackson, Ph.D. Dissertation, The University of Michigan (1980).
16. R. A. Warriner, *Solid-St. Electron Dev.* **1**, 105 (1977).
17. R. W. H. Englemann and C. A. Liechti, *Proc.* 1976 *Int. Electron. Devices Meeting*. 351 (1976).
18. H. Fukui, *Bell Syst. Tech. J.* **58**, 771 (1979).
19. H. H. Berger, *Solid-St. Electron.* **15**, 145 (1972).
20. R. A. Pucel, H. A. Haus and H. Statz, *Advances in Electronics and Electron Phys.* **38**, 195 (1975).
21. T. Wada and J. Frey, *IEEE Trans Electron Dev.* **ED-26**, 476 (1979).
22. C. Li, P. T. Chen and P. H. Wang, *Gallium Arsenide and Related Compounds*, Edited by C. M. Wolfe. 1978. The Institute of Physics, Conf. Series, No. 45, London, 353 (1979).
23. H. M. Macksey, R. L. Adams, D. N. McQuiddy, Jr., D. W. Shaw and W. R. Wisseman, *IEEE Trans Electron Dev.* **ED-24**, 113 (1977).
24. J. L. Lions and E. Magenes, *Non-Homogeneous Boundary Value Problems and Applications*. Springer-Verlag, Berlin (1972).

APPENDIX

The following norms are used; their definitions are standard [3] Chap. 2 and [24]. All distances are explicitly normalized to the average domain edge length $h^* \triangleq [\text{area } (\Omega)]^{1/2}$. Let $u(x, y)$ be a function in a two-dimensional domain Ω. Then:

1. $\|u\|_{L^\infty(\Omega)} = \|u\|_{L^\infty} \triangleq \sup_{x,y\in\Omega} |u|$.

2. $\|u\|_{L^2(\Omega)} = \|u\|_{L^2} \triangleq (h^*)^{-1}\left(\int\int_\Omega |u|^2 \, dx\, dy\right)^{1/2}$.

3. $\|u\|_{W_2^1(\Omega)} = \|u\|_{W_2^1}$

$$\triangleq \left[\|u\|_{L^2}^2 + \int\int_\Omega \left(\left|\frac{\partial u}{\partial x}\right|^2 + \left|\frac{\partial u}{\partial y}\right|^2\right) dx\, dy\right]^{1/2}.$$

Definition 3 can be extended to the case $\|u\|_{W_2^k}$, $k > 1$; see [3] Chap. 2 and [24]. In both [3, 24], our $W_2^k(\Omega) \equiv H^k(\Omega)$. Note, $\|u\|_{L^\infty} < \infty \Leftrightarrow u \in L^\infty$; similar for L^2 and W_2^k.